Characterization of the optical properties of atmospheric aerosols in Amazônia from long-term AERONET monitoring (1993–1995 and 1999–2006)

J. S. Schafer,[1,2] T. F. Eck,[2,3] B. N. Holben,[2] P. Artaxo,[4] and A. F. Duarte[5]

Received 23 August 2007; revised 13 November 2007; accepted 11 December 2007; published 21 February 2008.

[1] We present a new climatology of atmospheric aerosols (primarily pyrogenic and biogenic) for the Brazilian tropics on the basis of a high-quality data set of spectral aerosol optical depth and directional sky radiance measurements from Aerosol Robotic Network (AERONET) Cimel Sun-sky radiometers at more than 15 sites distributed across the Amazon basin and adjacent Cerrado region. This network is the only long-term project (with a record including observations from more than 11 years at some locations) ever to have provided ground-based remotely-sensed column aerosol properties for this critical region. Distinctive features of the Amazonian area aerosol are presented by partitioning the region into three aerosol regimes: southern Amazonian forest, Cerrado, and northern Amazonian forest. The monitoring sites generally include measurements from the interval 1999–2006, but some sites have measurement records that date back to the initial days of the AERONET program in 1993. Seasonal time series of aerosol optical depth (AOD), Ångström exponent, and columnar-averaged microphysical properties of the aerosol derived from sky radiance inversion techniques (single-scattering albedo, volume size distribution, fine mode fraction of AOD, etc.) are described and contrasted for the defined regions. During the wet season, occurrences of mineral dust penetrating deep into the interior were observed.

Citation: Schafer, J. S., T. F. Eck, B. N. Holben, P. Artaxo, and A. F. Duarte (2008), Characterization of the optical properties of atmospheric aerosols in Amazônia from long-term AERONET monitoring (1993–1995 and 1999–2006), *J. Geophys. Res.*, *113*, D04204, doi:10.1029/2007JD009319.

1. Introduction

[2] The Amazon basin is a key ecosystem in the global climate system, and one which is under particular stress from anthropogenic activities, especially deforestation which began to reach substantial levels in the mid-1970s and has continued unabated to the current day [*Andreae et al.*, 2002]. The Amazon represents the largest continuous rain forest in the world, and much attention has been devoted to studying the widespread deforestation by agricultural clearing and man-made fires and the impact of biomass burning aerosols on nucleation processes and cloud microphysics [*Andreae et al.*, 2004]. The annual biomass burning events result in significant seasonal aerosol loadings over vast stretches of the basin that are both pervasive and persistent during the dry season [*Holben et al.*, 1996], and as such, the Amazon is considered one of the primary sources of aerosol particles globally. Recently, additional focus has been placed upon studies conducted during the wet season and the transitional period between the seasons with an emphasis on cloud condensation nuclei concentration measurements and examining aerosol aging and humidification processes to improve regional precipitation models [*Mircea et al.*, 2005; *Rissler et al.*, 2006; *Falkovich et al.*, 2005; *Silva Dias et al.*, 2002].

[3] Aerosol radiative forcing is an area of keen scientific interest because it is a key parameter in understanding the perturbations that drive the climate system. The radiative effects of aerosols are conventionally broken down conceptually with terminology that distinguishes the mechanism by which the influence of the aerosol is manifested. The most basic forcing is simply that of the modification of net fluxes by scattering and absorption processes, referred to as the direct effect. Such forcing may be defined for the top of the atmosphere or at the surface and is calculated as the difference between net fluxes assessed with and without aerosol loading in the atmosphere. Semidirect effects result from increases in atmospheric stability due to heating of the troposphere by absorbing aerosols and reduction of solar flux at the surface, thereby causing clouds to evaporate or suppressing cloud formation [*Koren et al.*, 2004]. The

[1]Science Systems and Applications, Inc., Lanham, Maryland, USA.
[2]Biospheric Sciences Branch, NASA Goddard Space Flight Center, Greenbelt, Maryland, USA.
[3]Goddard Earth Sciences and Technology Center, University of Maryland Baltimore County, Baltimore, Maryland, USA.
[4]Departamento de Física Aplicada, Instituto de Física da Universidade de São Paulo, São Paulo, Brazil.
[5]Departamento de Ciencias da Natureza, Universidade Federal do Acre, Rio Branco, Brazil.

Copyright 2008 by the American Geophysical Union.
0148-0227/08/2007JD009319

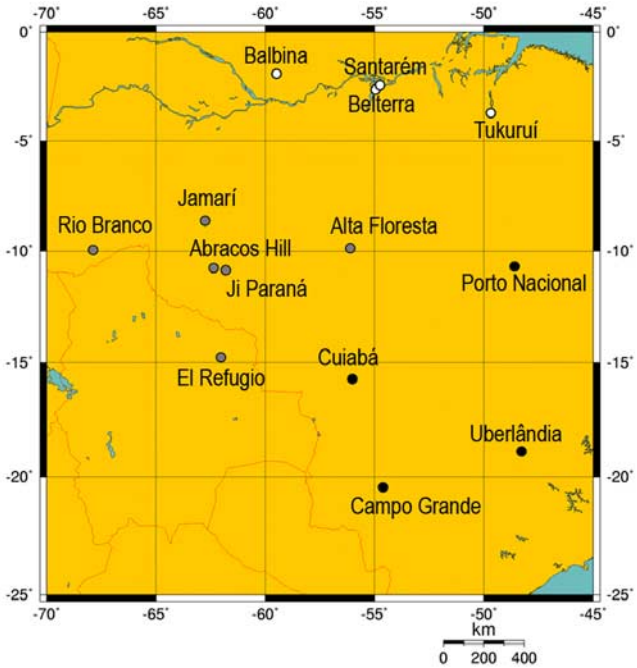

Figure 1. Locations of AERONET aerosol monitoring sites used in this study (white symbols, northern forest; gray symbols, southern forest; black symbols, Cerrado).

indirect effects of aerosols have much greater uncertainties [*Anderson et al.*, 2003] and include derivative consequences such as changes in cloud optical depth, albedo, and precipitation efficiency (and thus cloud lifetime) as well as alterations in the atmospheric stability due to heating of the troposphere by absorbing aerosols. Although the theoretical understanding of these indirect effects is well founded, evaluation of the magnitudes is subject to significant uncertainties resulting from large spatial and temporal variability of aerosols [*Chylek et al.*, 2003].

[4] With the exception of Aerosol Robotic Network (AERONET), there is a dearth of historical, systematic ground-based measurements of column-integrated aerosol optical properties because of constraints imposed by instrument maintenance and calibration requirements [*Liu et al.*, 2005], particularly in the developing region of the world [*Jethva et al.*, 2005]. Efforts to establish aerosol databases via satellite-based aerosol characterization as well as aerosol source and transport models have been increasingly successful [*Yu et al.*, 2003; *Kinne et al.*, 2003], however, most have dependencies upon aerosol parameterization assumptions derived from networks such as AERONET. Detailed analyses of high-quality observations of aerosol microphysical and optical properties from long-term AERONET monitoring sites can yield a complete characterization of aerosol optical effects for a wide range of applications.

2. Site Descriptions and Background

[5] The Brazilian sites (plus one Bolivian site, i.e., El Refugio) can be organized into three regional groups: southern Amazonian forest, southern Cerrado (woodland/savanna), and northern Amazonian forest. Figure 1 shows the location of every site that has contributed data to this study since 1993, and the color of the marker indicates the regional group within which the site belongs (white symbols, northern forest; black symbols, Cerrado; gray symbols, southern forest).

[6] The AERONET conducted its first large-scale deployments outside the continental United States beginning in 1993 with a campaign based on eight monitoring sites in the Amazon [*Holben et al.*, 1998, 2001]. This and subsequent deployments to Brazil in 1994 and 1995 were largely seasonal campaigns focused on characterizing the heavy aerosol loading associated with forest fires during the dry season [*Holben et al.*, 1996; *Eck et al.*, 1998]. From these origins the project has expanded to include hundreds of sites around the world, and after a period of absence from Brazil, resumed year-round monitoring at multiple locations in 1999 in conjunction with a component of the Large-Scale Biosphere Atmosphere (LBA) project.

[7] A Cimel Sun-sky radiometer is deployed at each site and six sites also include a Kipp & Zonen CM-21 Pyranometer (305–2800 nm) for measuring the global solar flux in the total solar spectrum. The automatic Sun-sky radiometers (model CE318A) were manufactured by Cimel Electronique and their characteristics are discussed at length by *Holben et al.* [1998]. Each is equipped with narrow bandpass filters in the visible and near infrared with center wavelengths at 340, 380, 440, 500, 675, 870, 940, and 1020 nm. The filters are ion-assisted deposition interference filters with bandpass (full width at half maximum) of 2 nm for the 340 and 380 nm channels and 10 nm for all other channels. The Cimel Sun-sky radiometer measures aerosol optical depth (AOD) at each of these wavelengths, except for the 940 channel which is used to derive total column water vapor (CWV). The uncertainty in measured AOD, due primarily to calibration uncertainty, is approximately 0.010–0.021 for field instruments (which is spectrally dependent with higher errors in the UV [*Eck et al.*, 1999]). The spectral AOD data have been screened for clouds following the methodology of *Smirnov et al.* [2000], which relies on the greater temporal variability of cloud optical depth versus aerosol optical depth. In addition to the direct Sun irradiance measurements that are made with a field of view of 1.2° these instruments measure the sky radiance in four spectral bands (440, 670, 870, and 1020 nm) along the solar principal plane (i.e., at constant azimuth angle with varied view zenith angles) up to nine times a day and along the solar almucantar (i.e., at constant solar zenith angle with varied view azimuth angles) up to eight times a day (for solar zenith angle greater than 45°). A preprogrammed sequence of measurements is taken by these instruments starting at an air mass of seven in the morning and ending at an air mass of seven in the evening. During the large air mass periods direct Sun measurements are made at 0.25 air mass intervals, while at smaller air masses the interval between measurements is typically 15 min. The almucantar measurements are taken at 0.5° azimuth angle intervals near the Sun (within 6°) and increase from 2 to 10° intervals away from the solar position. It is these sky radiance measurements that are used to retrieve additional column aerosol properties including volume size distribution, phase function, real and imaginary component of refractive index, effective radius, and single-scattering albedo (SSA)

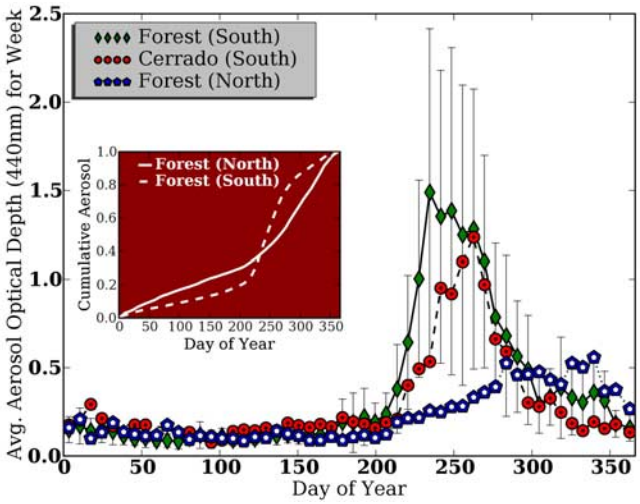

Figure 2. Weekly averages of aerosol optical depth (440 nm) for regionally grouped sites and cumulative aerosol contribution (inset).

that are routinely computed with the AERONET inversion algorithms [*Dubovik and King*, 2000; *Dubovik et al.*, 2006]. The almucantar radiance inversion technique for determining both the real and imaginary refractive indices is most accurate when AOD at 440 nm is greater than 0.4 [*Dubovik et al.*, 2000], solar zenith angle is larger than 50°, and the sky-radiance-fitting error is less than 5–8%, dependent on AOD [*Holben et al.*, 2006]. Therefore Cimel inversion products such as single-scattering albedo used in this study were restricted to those that met the above criteria, resulting in SSA uncertainty of approximately 0.03 or less (uncertainty decreases as AOD increases).The changes in sky radiance processing and quality criteria implemented for the version 2 inversions are detailed by *Holben et al.* [2006].

3. Aerosol Optical Depth and Column Water Vapor Seasonal Cycles

3.1. Regional Aerosol Comparison

[8] Figure 2 shows weekly averages for composite data sets that combine the observations from all sites within a given regional group. These weekly values are an average of all qualifying day averages from the given week and so the standard deviation bars include variation due to both interannual and intersite variation. Additionally, monthly averages of AOD and Ångström exponent are presented in Table 1. The majority of the data contributed from the original study years (1993–1995) are for the burning season periods, since the early campaign deployments were preferentially conducted during these intervals. Therefore there are typically many more day averages available in the July–October months, although the much smaller variability in observed AOD during the wet season period means that the lower number of observations is still quite suitable to characterize the AOD tendencies. Given the intermittent deployments of some of the secondary sites and the longer data record dating to 1993 for Alta Floresta and Cuiabá, the observations from these two sites are represented disproportionately in their respective regional composite data sets. Alta Floresta contributes approximately 40% of the data for the southern forest region, and Cuiabá is responsible for more than 60% of the Cerrado measurements.

[9] All sites exhibit a broadly similar seasonal cycle in atmospheric conditions with a relatively cloudy low-background aerosol regime in effect during the Southern Hemisphere winter and spring (January–June). As the year progresses, a much drier interval manifests itself with an associated large increase in aerosol optical depth as biomass burning activities become prevalent. The magnitude of this seasonal variation in column water vapor is more pronounced in the southern Amazon, and the intensity and extent of the biomass burning is significantly greater. The northern Amazon is found to experience its peak AOD levels later in the year (October) than is observed in the south (September) due to a later dry season peak.

[10] In the inset plot of Figure 2, the slope of each line depicting the average cumulative aerosol loading is proportional to the contribution of a given day to the total aerosol for the year and it can be seen that the southern forest region exhibits a greater degree of seasonality in AOD than the northern region. For the southern forest, 60% of the annual aerosol loading is produced during the period from mid-August to September (day range is 225–275).

[11] The monthly average AOD (440 nm) values are very similar in all regions during the first half of the year with consistent background low-aerosol conditions (approximately 0.1–0.15), and the averages for the north and south

Table 1. Monthly Averages and Standard Deviation of Aerosol Optical Depth (440 nm) and Ångström Exponent (440/870 nm) Grouped by Region

	AOD 440 Northern Forest	SD Northern Forest	AOD 440 Southern Forest	SD Southern Forest	AOD 440 Cerrado	SD Cerrado	Angström Exponent Northern Forest	SD Northern Forest	Angström Exponent Southern Forest	SD Southern Forest	Angström Exponent Cerrado	SD Cerrado
Jan	0.16	0.09	0.15	0.08	0.22	0.14	0.88	0.35	1.09	0.45	0.79	0.31
Feb	0.12	0.06	0.11	0.06	0.17	0.10	0.62	0.33	0.90	0.45	0.83	0.30
Mar	0.14	0.08	0.10	0.06	0.12	0.05	0.65	0.34	0.96	0.46	1.05	0.52
Apr	0.10	0.06	0.10	0.05	0.12	0.06	0.73	0.37	1.11	0.50	1.13	0.41
May	0.12	0.06	0.12	0.05	0.16	0.05	0.84	0.31	1.33	0.42	1.02	0.31
Jun	0.10	0.04	0.14	0.08	0.19	0.21	1.07	0.30	1.40	0.39	1.00	0.43
Jul	0.12	0.05	0.23	0.17	0.18	0.12	1.18	0.37	1.54	0.34	1.11	0.43
Aug	0.22	0.11	1.03	0.78	0.52	0.49	1.20	0.39	1.87	0.24	1.42	0.41
Sep	0.32	0.16	1.24	0.80	1.03	0.66	1.14	0.33	1.69	0.33	1.65	0.23
Oct	0.47	0.27	0.62	0.40	0.51	0.35	1.23	0.34	1.54	0.37	1.44	0.43
Nov	0.46	0.26	0.33	0.21	0.26	0.18	1.28	0.35	1.26	0.43	0.91	0.53
Dec	0.40	0.25	0.26	0.17	0.16	0.08	1.05	0.37	1.12	0.46	0.80	0.48

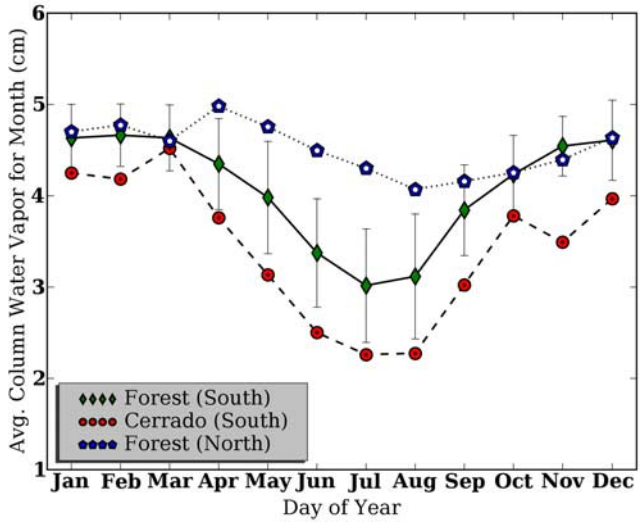

Figure 3. Monthly averages of column water vapor for sites grouped by region.

differ by less than 0.05 for any given month. The onset of the burning season leads to dramatic increases in AOD, particularly in the south, with the September average AOD for the southern forest region (1.25) that is approximately 3.5 times greater than the comparable average in the northern forest region (0.35) and represents an order of magnitude increase over the wet season month averages. The pattern of seasonal AOD for the Cerrado region is similar to that of the southern forest region, though the magnitude of AOD is less and the peak delayed by about 25 days, with early burning season averages that are typically approximately 75% of those for the corresponding months at the forest sites.

[12] Column water vapor monthly averages for each region are presented in Figure 3 and are consistent with what might be expected from the observed AOD seasonality, since rainfall is somewhat associated with the seasonal water vapor cycle. The two southern regions exhibit the smallest CWV values and the largest seasonal variability with annual ranges of approximately 1.5 cm and standard deviations of 0.35–0.8 cm. The two predominantly forested regions have comparable water vapor amounts during the wet season, but the equatorial northern forest exhibits much less decrease in CWV over the course of the year (approximately 0.6 cm), with standard deviations that are more consistent from month to month (0.3–0.4 cm). The CWV record for the Cerrado sites in this study are notably lower than even the southern forest region and remain so throughout the season.

[13] The CWV measurements from the Cimel Sun photometer have been compared to several different sources to assess accuracy, including radiosondes [*Halthore et al.*, 1997] and various other radiometers such as the Ames Airborne Tracking Sun Photometer (AATS-6), Multifilter Rotating Shadowband Radiometer, and a microwave radiometer at the Great Plain Atmospheric Radiation Measurement site [*Schmid et al.*, 2001]. *Halthore et al.* [1997] reported an agreement of ±10% between Cimel and radiosonde measurements, while Schmid et al. found an RMS difference in CWV measurements from the AATS-6 and Cimel of 0.08 cm (3.2%) when using the same water vapor spectral profile. Recently, after refining the Cimel algorithm to use exact filter functions for each instrument the record of Cimel precipitable water vapor measurements were observed to be in good agreement (RMS difference is 0.15 cm (7.0%)) with CWV measurements derived from

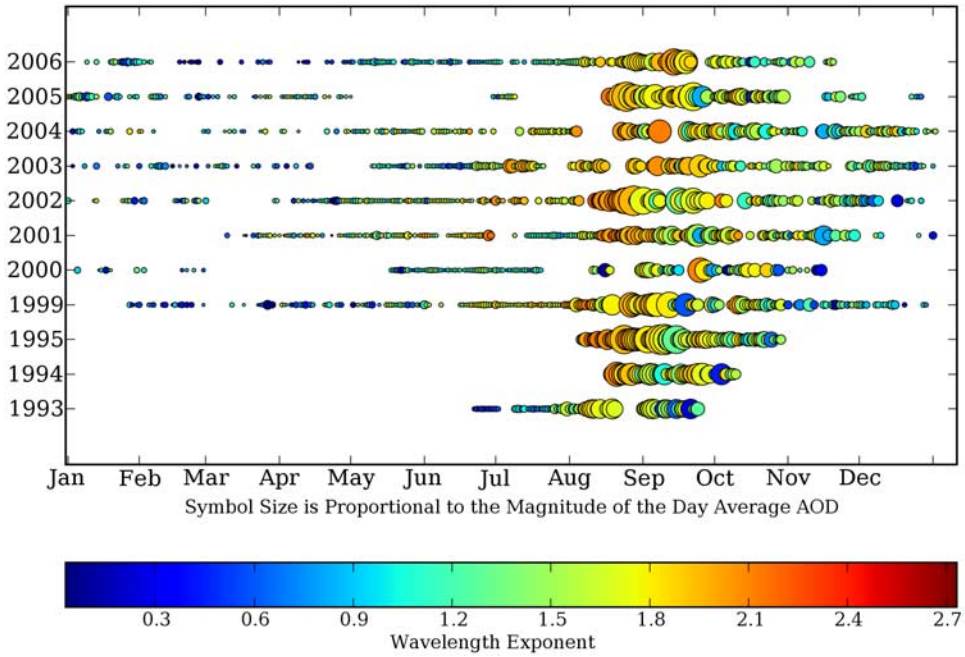

Figure 4. Multiyear record of aerosol optical depth (440 nm) at Alta Floresta. Symbol size is proportional to AOD and the color indicates the Ångström exponent.

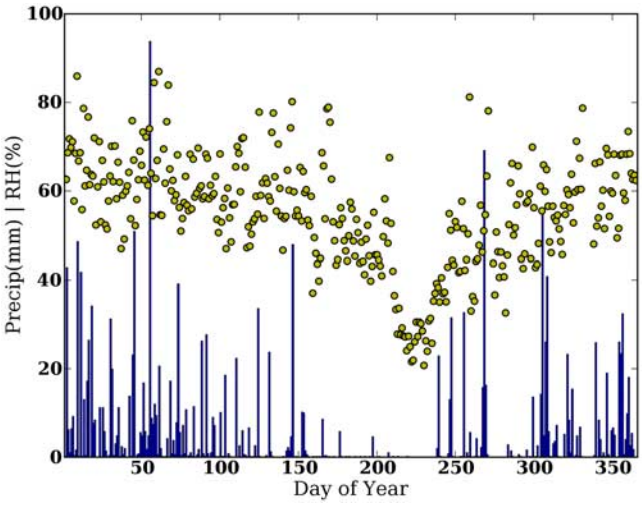

Figure 5. Day-averaged precipitation and daily minimum relative humidity for a southern forest site (Abracos Hill data from 2001) (precipitation and relative humidity data provided courtesy of David Fitzjarrald and the Atmospheric Sciences Research Center, University of Albany).

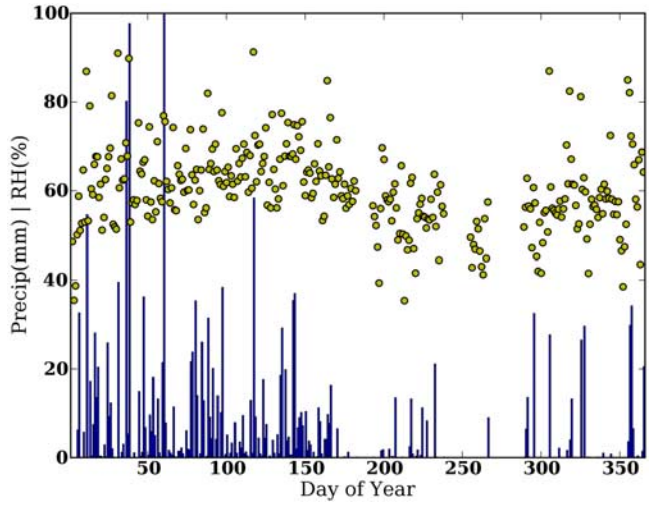

Figure 6. Day-averaged precipitation and daily minimum relative humidity for a northern forest site (Belterra data from 1999) (precipitation and relative humidity data provided courtesy of David Fitzjarrald and the Atmospheric Sciences Research Center, University of Albany).

GPS receivers during a multiyear comparison at the Goddard Space Flight Center (GSFC) [*Smirnov et al.*, 2004].

[14] The timing of the onset of fire activity in the Amazon is of course tied to the local meteorological cycle, though the beginning of the burning is relatively consistent from year to year, usually varying by only a few weeks. An example of this can be seen in Figure 4 where the record of AOD measurements at Alta Floresta is broken out by year. The size of each point is proportional to the magnitude of the daily averaged AOD and the scale bar on the bottom can be used to determine the Ångström exponent for the day based on the data point's color level. The precipitation minimum of the dry season cycle is also reflected in the relative humidity (daily minimum) and produces the environmental conditions favorable for initiating biomass burning (example years shown in Figures 5 and 6). The dry season is observed to be more pronounced for the southern forest sites (Abracos Hill data from 2001 (Figure 5)) than for the northern forest site (Belterra data from 1999 (Figure 6)), though the consistent association of rainfall and AOD is evident (precipitation and relative humidity data provided courtesy of David Fitzjarrald and the Atmospheric Sciences Research Center, University of Albany).

[15] Figures 7 and 8 depict the interannual variability of day-averaged AOD for typical southern (Alta Floresta) and northern (Belterra) forest sites and illustrate the effect of year-to-year variation of factors that influence biomass burning aerosol production. For the day range from 150 to 300 each point is typically based on daily AOD averages from 5–11 different years at Alta Floresta. The shaded bands indicate the approximate starting and ending months of the respective burning seasons. The interannual variability is obviously greatest during the respective burning seasons in each site with the southern forest site exhibiting larger relative variance (mean value of $AOD_{std(day)}/AOD_{avg(day)}$ for the burning season is 0.55) than does the northern forest site (0.43). The corresponding values for the southern and northern sites during the rest of the year (nonburning) are 0.42 and 0.31, respectively. The biomass burning in the northern region begins more gradually than in the south because of a dry season that is less severe in this area. The plotted values for the wet season (first months of the year) at the Belterra site are more scarce because of the consistent cloud cover that limits aerosol measurement opportunities and because the persistently rainy conditions have made instrument failure more common during these intervals. Points with center marks represent cases where only a single day-averaged AOD was available for the day of interest (i.e., there is a day-averaged AOD from one year only) and so no interannual standard deviation can be calculated. The aerosol loading on a given day during a particular burning season is a result of such contingencies as

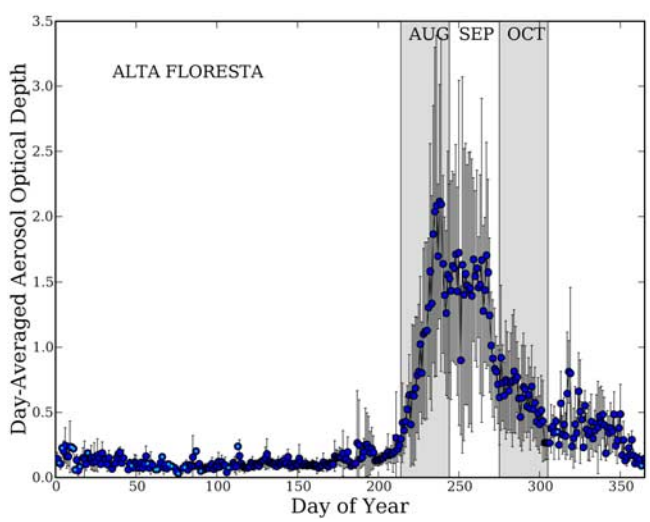

Figure 7. Time series and interannual variability of day average AOD (440 nm) for Alta Floresta (11 years).

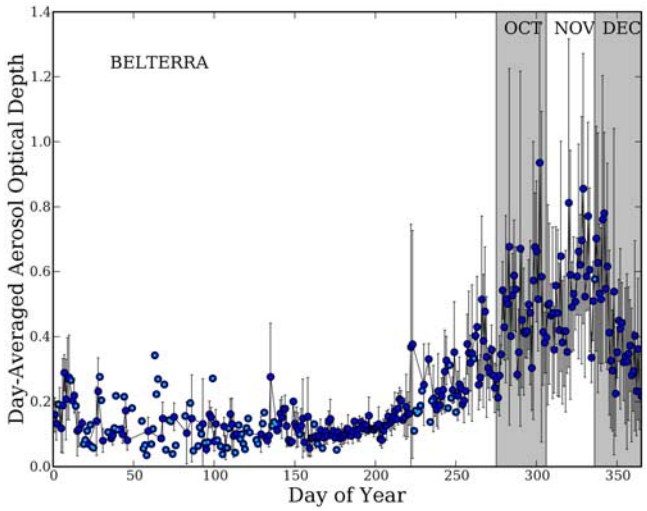

Figure 8. Time series and interannual variability of day average AOD (440 nm) for Belterra (5 years).

the severity of the dry season, onset date of burning, local fire management policies, regional meteorology, and transport tendencies as well as other factors that are difficult or impossible to predict.

3.1.1. Aerosol Optical Depth Histograms

[16] Relative frequency histograms of aerosol optical depth during the respective burning season at two sites (August–October for Alta Floresta (Figure 9) and October–December for Belterra (Figure 10)) show the greater interannual variability of the southern forest sites. At Alta Floresta, the data record for 2000 was not as complete during the burning season months and was not included in the plot. Burning season AOD_{440} averages can vary by a factor of 2.5 from year to year (0.6–1.5) as do the more extreme events as indicated by the average value of the top 10% of measurements shown in parentheses (range is 1.59–3.92). The occurrence of measurements during very high aerosol loading ($AOD_{440} > 2.0$) as a percentage of the total number ranges from a low of 1% in 2001 to greater than 20% for intense burning years such as 2002 and 2005.

[17] By contrast the northern histograms are fairly uniform in appearance with relatively little difference in AOD averages and similar frequency distributions for all 5 years on record. This may in part be due to less variation in the intensity of the dry seasons in the north.

3.1.2. Wavelength Dependence of Aerosol Optical Depth

[18] Plots of interannual variability of the wavelength dependence of AOD, as characterized by the Ångström exponent (based on two wavelengths, i.e., 440 and 870 nm) α, are presented for Alta Floresta, Belterra, and Cuiabá (Figures 11–13).

[19] The salient feature of the Alta Floresta plot is the peak of α during a week around the middle of August (approximately day 225). The Ångström exponent is highly sensitive to the size distribution with larger values encountered when the fine mode aerosol has a large relative contribution to the total aerosol. This peak appears near the start of the burning season when there is a combination of minimal cloud presence and initial fire activity and is assumed to be a period of nearly pure smoke aerosol with perhaps more fresh smoke and less contribution from aged

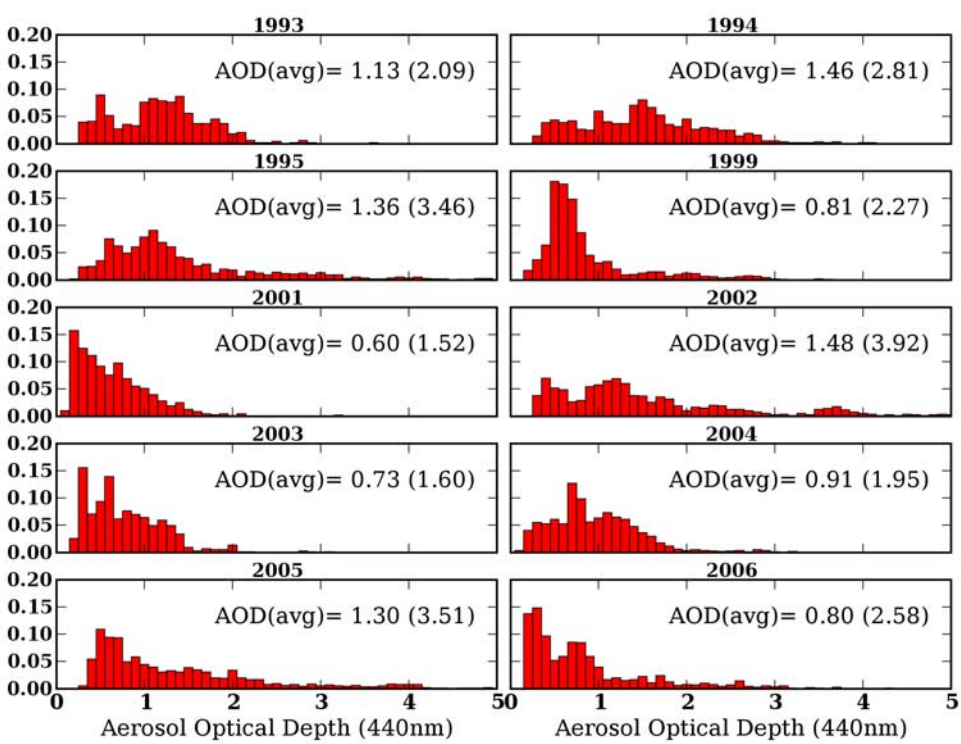

Figure 9. Relative frequency histograms of aerosol optical depth (440 nm) during the burning season for 10 years at Alta Floresta.

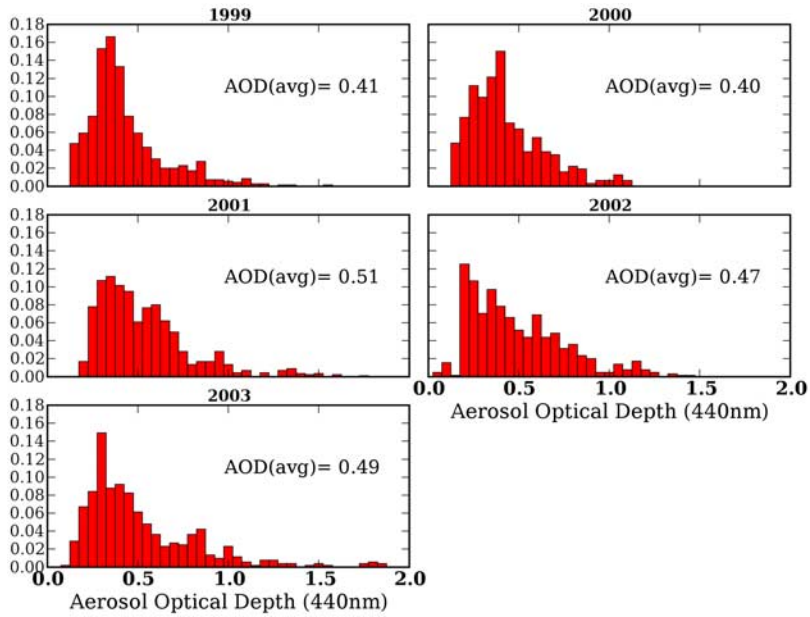

Figure 10. Relative frequency histograms of aerosol optical depth (440 nm) during the burning season for 5 years at Belterra.

smoke as would be expected later in the burning season. The Ångström exponent can vary by a factor of nearly 2 for aged versus fresh smoke cases but also because of fuel type and combustion phase [*Eck et al.*, 2003]. The consistently high value of α during this week is remarkable with negligible variability shown despite the fact that this interval includes observations from as many as 11 different years. The Ångström exponent remains high after this period, but the typical enhancement of convective activity introduces some inevitable cloud contamination that reduces the average α slightly. This eventual reduction might also be due in part to the effects of more aged aerosol and a greater percentage of smoldering combustion later in the burning season that results in larger size accumulation mode particles that would also decrease the Ångström exponent.

[20] The pattern is similar for the Cerrado site, Cuiabá (Figure 13), though this region is typically dryer and sunnier and also may have more consistency in fuel type burned and combustion mode fraction (smoldering/flaming). The Ångström exponent remains elevated longer than at Alta Floresta, commonly averaging greater than 1.6 for the whole month of September, though the peak value of α is higher for Alta Floresta than the corresponding peak at Cuiabá. The Ångström exponent is also observed to increase during the biomass burning season at Belterra but less prominently. This is partially due to lower AODs since the background

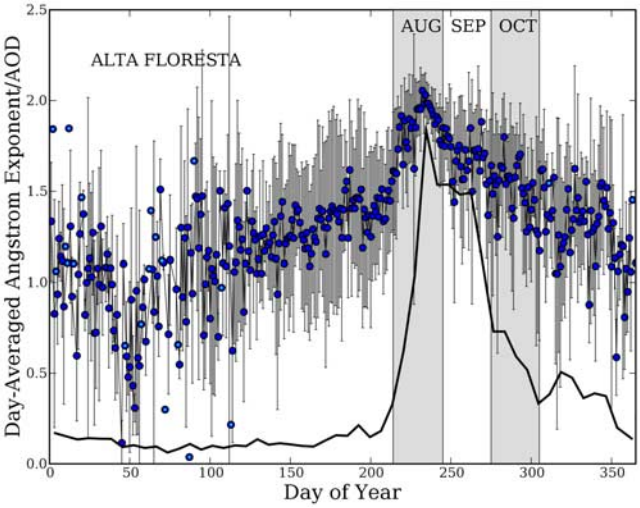

Figure 11. Time series and interannual standard deviation of day average Ångström exponent (440/870 nm) for Alta Floresta (11 years). The time series of weekly average AOD (440 nm) is also shown (black line).

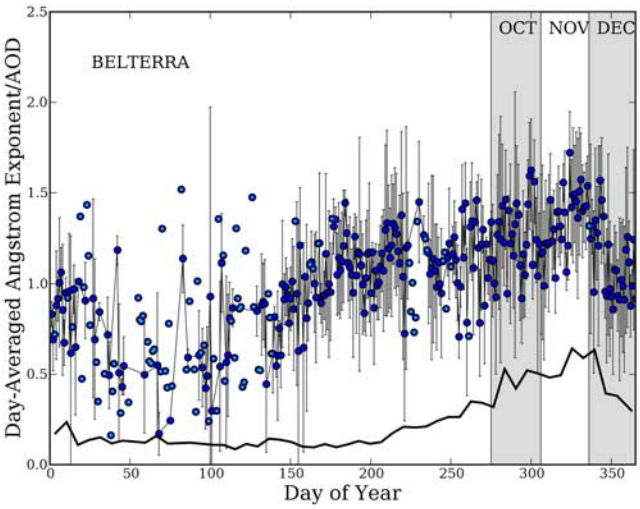

Figure 12. Time series and interannual standard deviation of day average Ångström exponent (440/870 nm) for Belterra (5 years). The time series of weekly average AOD (440 nm) is also shown (black line).

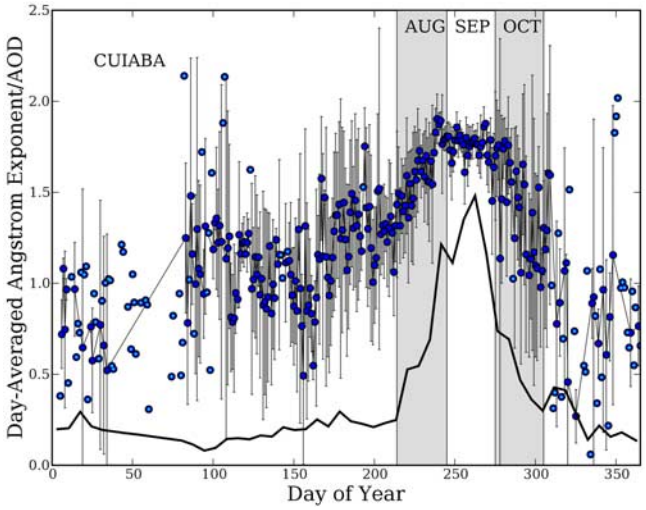

Figure 13. Time series and interannual standard deviation of day average Ångström exponent (440/870 nm) for Cuiabá (9 years). The time series of weekly average AOD (440 nm) is also shown (black line).

coarse mode AOD has a greater influence on the Ångström exponent, as shown by the observation that α increases as AOD increases for smoke aerosols [*Eck et al.*, 2001]. Another factor that might have resulted in lower α at Belterra is a possibly greater contamination in the northern Amazon by clouds (which are more abundant there than is the case for the southern Amazon during the dryer months).

3.2. Ångström Exponent and Cloud Contamination Effects

[21] Additional evidence of minor cloud effects upon the derived Ångström exponent is provided by comparing the data set of this parameter acquired from all direct Sun measurements with those acquired only during the almucantar sequence. Figure 14a depicts the time series of α for the June–October interval in the southern forest region and the observed differences in α for the two data sets may be indicative of the influence of clouds. Each point represents the multiyear average of all available day-averaged α for the given day of year, and only days with at least 5 different years of day averages were included. Since the almucantar coincident α values are limited to those derived from almucantar procedures with low retrieval errors, they are necessarily drawn from observations taken during conditions where the sky radiances are considered free of cloud cover within the majority of the almucantar scan view angles (and which have also passed the standard AOD triplet variability and time series variability checks). This should serve to produce a data set that is less prone to exhibit effects because of clouds than the Ångström exponent measurement data set derived from all direct Sun only

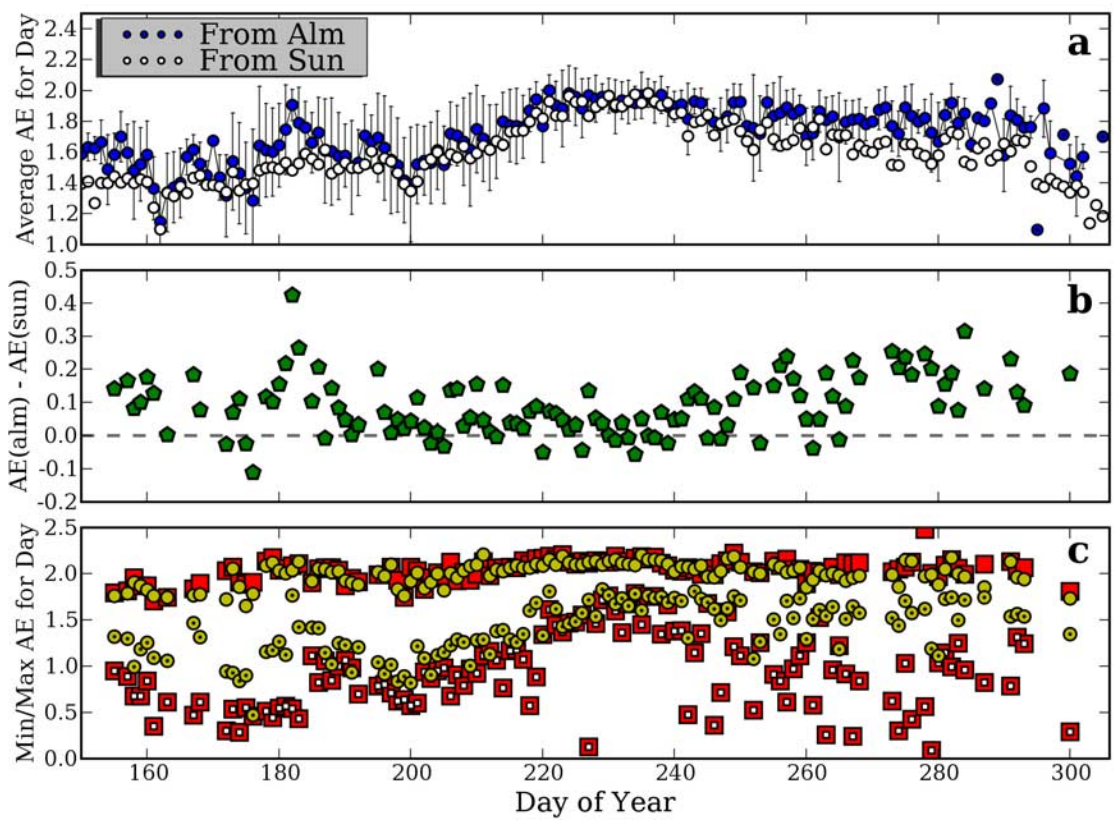

Figure 14. (a) Time series of α (440/870 nm) for the June–October interval in the southern forest region derived from almucantar and direct Sun measurements. (b) Computed mean difference between the day-averaged α for each day of year. (c) Time series of minimum (center-marked symbols) and maximum (open symbols) observed day-averaged α derived from almucantars (circles) and direct Sun measurements (squares).

observations, even though all the data are thoroughly screened for clouds as part of the standard protocol. Figure 14b presents the computed mean difference between the day-averaged α for each day of year. It is apparent that the Ångström exponents (from direct Sun measurements) associated with the almucantar measurement sequence are higher (approximately 0.1 on average) than those based on the average of all direct Sun measurements. Although the day average Ångström exponent for the almucantars is limited to solar zenith angles greater than 45°, while the day average for the direct Sun measurements include observations throughout the day, it was found that there was no bias introduced by including the midday Ångström exponents measurements for only one data set, i.e., there was no diurnal dependence to the Ångström exponent in the direct Sun measurements that might produce the discrepancies that were observed.

[22] Further, the difference appears to be positively correlated with the degree of cloudiness with almost no discrepancy in evidence during the least cloudy interval beginning around day 225. In part, the assessment of general cloudiness (cloud frequency) was based on in situ broadband flux measurements (2-min sampling) which have been operated at the site for the duration of the project. We have cloud-screening algorithms for the flux based on comparisons with several radiative transfer models [e.g., *Vermote et al.*, 1997] which allow us to evaluate which months are associated with minimal cloud fractions, and also, broadly speaking, the seasonal tendencies of cloud cover are consistent and known well enough to make general statements about which parts of the year are more frequently cloud free than others.

[23] Additional investigation supports the speculation that this is due to cloud contamination. If for each day of the year the maximum and minimum day values of α included in the multiyear average are examined (Figure 14c), it is observed that the maximum values are quite similar for both data sets (almucantar average is 2.01 and direct Sun is 2.04), while the minimum values are much lower on average for the direct Sun measurements (average is 0.95) than for the almucantar-associated measurements (average is 1.39). This may suggest that the discrepancy is not systematic but rather an intermittent (but possibly not uncommon) contamination effect, at least for locations experiencing certain types of cloud cover. When other long-term monitoring sites are examined, the same effect is observed (a diminished average minimum Ångström exponent for direct Sun measurements is found), and additionally, the magnitude appears smaller at less cloudy locations. At one site with predominantly minimal cloud fraction, Sede Boker, Israel, the average difference of minimum α for the two data sets was only 0.08, compared to approximately 0.44 at Alta Floresta.

4. Multiyear Aerosol Optical Depth Analysis

[24] An investigation of long-term trends was performed for the site with the longest deployment record, Alta Floresta, which has burning season aerosol optical depth measurements for 11 years. The average AOD was computed for the August–October interval (calculated as the average of all day averages) for every year that had a largely complete measurement record during the burning season. These average AOD values were plotted versus the data year and included nine different years extending back to 1994. Despite increasing efforts at fire management in the Amazon over the last decade, we did not observe any trend in AOD that was significant at the 95% confidence level.

[25] Additionally, when AOD averages for individual week intervals are examined for all available data years (based on as many as 10 years for many week intervals), they are also found to exhibit no significant trend in aerosol optical depth over the data record. Of course this assessment represents only one point location and may not be representative of the basin at large, and the trend analysis is also diminished by the absence of measurements in the years from 1996–1998. If the same analysis is performed for the Cerrado site, Cuiabá, which has a record extending to 1993, there is a similar lack of any significant trend in AOD, although this site had only 6 years that possessed a sufficiently complete set of burning season measurements to meet our minimum requirements.

5. Aerosol Volume Size Distributions

5.1. Volume Median Radius and Aerosol Optical Depth

[26] Numerical inversion techniques applied to measured sky radiances from Cimel almucantars scans provide a means to retrieve columnar-averaged aerosol size distributions during favorable conditions (relatively cloud-free, spatially homogeneous sky). Figures 15 and 16 were generated by grouping the data from a southern forest site (Alta Floresta) and a Cerrado site (Cuiabá), respectively, into designated AOD ranges and averaging the retrieved size distributions within each aerosol bin. As noted in previous studies of smoke aerosol, each region exhibits an increase of fine mode (submicrometer) particles and a general shift toward larger volume median radius VMR_f for the accumulation mode as (smoke) aerosol optical depth increases. This has typically been attributed to the fact that the heaviest smoke conditions have larger aerosol concentrations which are more favorable for coagulation processes associated with "aging" smoke [*Reid et al.*, 1998, 1999]. For the Cuiabá site the larger fine mode volume radius retrievals for the lowest-AOD_{440nm} bin (AOD < 0.1) may be due to the influence of urban aerosols from the city (approximately 0.5 million people) rather than representative of predominantly biomass burning aerosols.

[27] Fine mode fraction (FMF) of the AOD represents the relative contribution of the fine mode to the total aerosol optical depth. In this context the fine/coarse mode threshold size is determined by calculating the inflection point between observed modes (but with the threshold always being constrained to the range of 0.44–0.99 μm). This parameter can be used as a general indicator of the presence of anthropogenic aerosol, which is predominantly found in the fine mode. In the case of Brazilian aerosols the higher FMF values are associated with biomass burning activities for land use purposes.

[28] For both regions the fine mode contribution to aerosol optical depth (as indicated by the fine mode fraction) is the dominant influence on the total AOD, amounting to approximately 80% of the attenuation even at the lowest

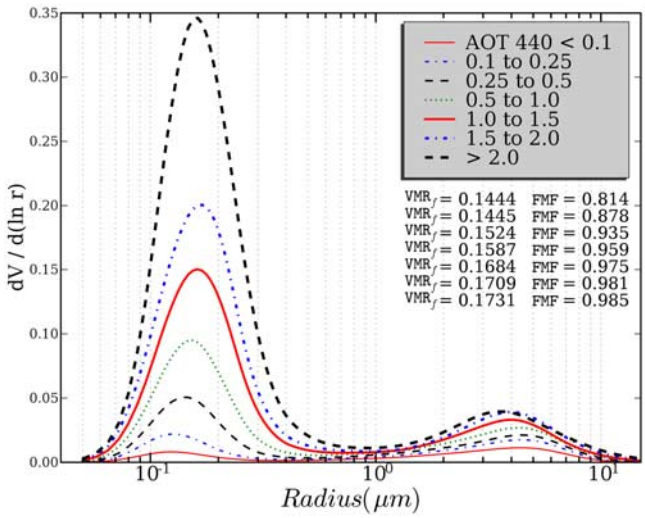

Figure 15. Retrieved aerosol volume size distributions for a southern forest site (Alta Floresta) averaged for each aerosol optical depth interval. Volume median radius of the fine mode (VMR_f) and fine mode fraction of AOD averaged for each AOD bin are also shown.

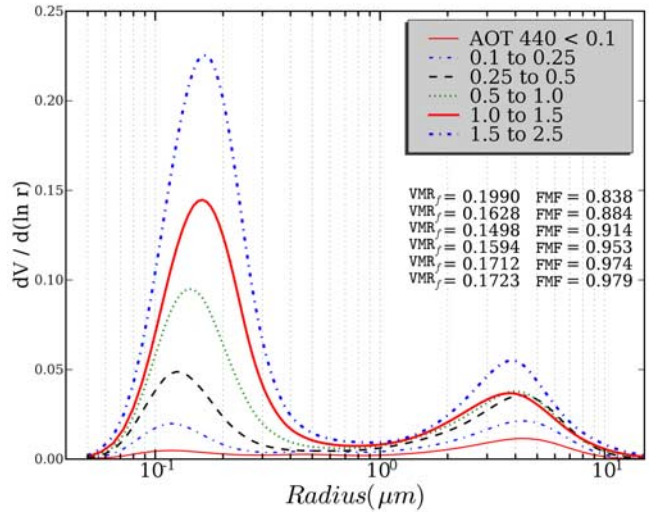

Figure 16. Retrieved aerosol volume size distributions for a Cerrado site (Cuiabá) averaged for each aerosol optical depth interval. Volume median radius of the fine mode VMR_f and fine mode fraction of AOD averaged for each AOD bin are also shown.

AOD. For the highest AOD the coarse mode is essentially optically negligible.

5.2. Column Water Vapor and Aerosol Particle Growth

[29] While column-averaged aerosol volume size distributions alone are not adequate to make quantitative assessments of hygroscopicity, they allow for useful inferences about this particular aerosol quality. Size distributions (fine mode only (Figure 17)) for the composite Amazonian southern forest sites were partitioned into two ranges of column water vapor. Such a study would ideally be done with relative humidity profile information, however, these data were not available and previous studies have found significant correlation between relative humidity and total column water vapor [*Raj et al.*, 2004]. The retrievals exhibit an increase of VMR_f as a function of AOD that was enhanced for the almucantars acquired during conditions of greater column water vapor. The volume size distributions in the submicrometer range are very similar for both low and high CWV for the lower-AOD bins, but as the aerosol loading increases, the separation between the two families of size distribution curves becomes steadily greater. During the LBA-SMOCC (Smoke Aerosols, Clouds, Rainfall, and Climate) campaign, *Rissler et al.* [2006] found the Amazonian (state of Rondônia) dry season (defined as 11 September to 8 October for the year of study, 2002) to be dominated by largely hydrophobic aerosol, while the transitional period (9–30 October) between the wet and dry season had an increasing influence of hydrophilic particles. In the Rissler et al. study, two largely distinct aerosol types were observed in all seasons, one nearly hydrophobic and the other moderately hygroscopic, and the overall effective hygroscopicity of the average aerosol in a given season was determined by the relative proportions of the number concentrations for each aerosol type. The almucantars in Figure 17 associated with the lowest CWV (1.5–2.5 cm) all occurred during the start of the burning season (August). However, even if only this early interval is considered, a similar stronger dependence of VMR_f on AOD for high CWV is observed when the almucantars are grouped into CWV bins, so by this assessment it is not evident that the difference in hygroscopic growth between the populations is related to changes in the ambient aerosol type (or changes in the relative contribution of different aerosol types) over the season. Nonetheless, the apparent hygroscopicity of the Amazonian biomass burning aerosol is quite modest compared to that observed for the typical urban aerosol of the eastern United States, as can be seen when the 3.5–4.5 cm CWV size distributions are plotted with the equivalent

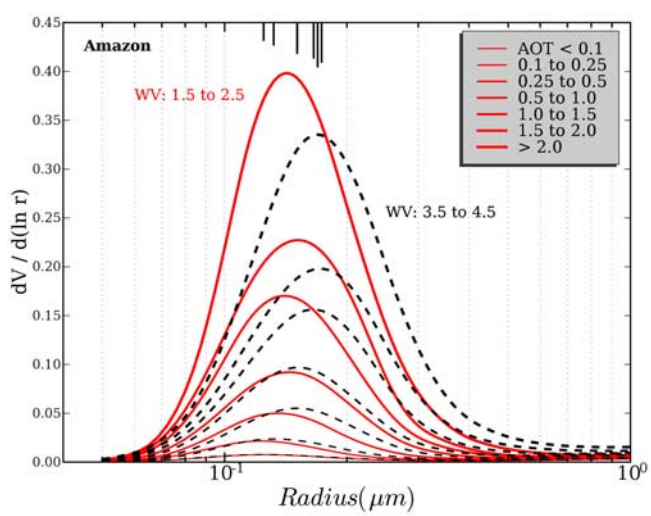

Figure 17. Averaged volume size distributions (fine mode only) grouped by aerosol optical depth for the composite Amazonian southern forest sites partitioned into two ranges of column water vapor.

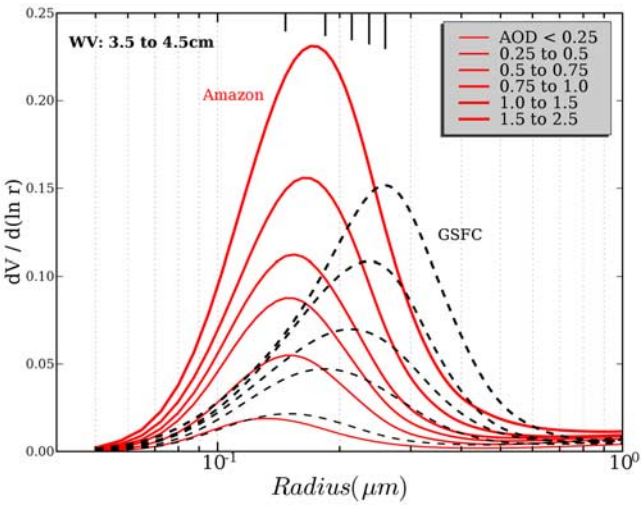

Figure 18. Averaged volume size distributions (fine mode only) grouped by aerosol optical depth for the composite Amazonian southern forest sites and for an urban aerosol (Goddard Space Flight Center) for all cases when the observed column water vapor was between 3.5 and 4.5 cm.

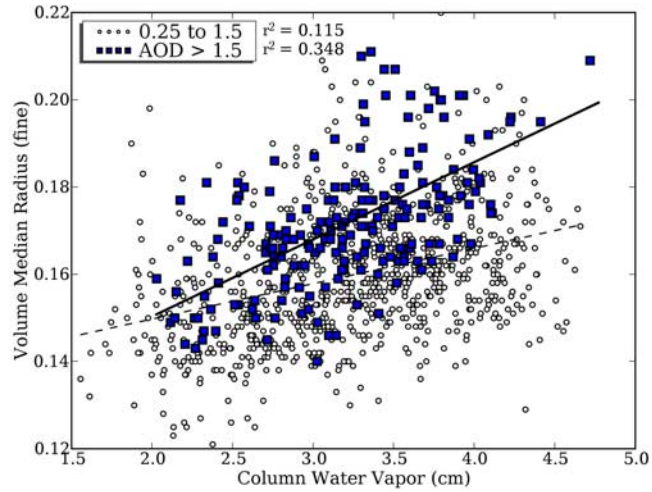

Figure 19. Volume median radius of the fine mode VMR_f as a function of column water vapor for two aerosol optical depth (440 nm) bins.

curves for the AERONET site at the GSFC in Figure 18. *Kotchenruther and Hobbs* [1998] similarly measured a much greater increase in light scattering coefficient at high relative humidity for United States east coast pollution as compared to biomass burning smoke in Brazil. A slightly different set of AOD bins were used because of the lower maximum AOD for the urban site. In each plot the large tick markers in the center of the upper axis indicate the corresponding sizes of the peak volume concentration for each of the dashed curves and ranged from 0.13 to 0.17 μm (from low to high AOD) for the higher-CWV bin in the Amazon for biomass burning aerosols, compared to a shift from 0.15 to 0.26 μm for the set of size distributions at GSFC for urban/industrial pollution aerosols.

[30] It was found that the sensitivity of VMR_f to CWV was dependent on the amount of aerosol (smoke) present. In Figure 19 volume mean radius (fine mode, VMR_f) was plotted versus column water vapor for moderate to high AOD_{440nm} (0.25–1.5; N = 825) and for very high AOD (greater than 1.5; N = 192) during the burning season (1 August to 15 October). The significance of the correlation and the regression slopes were notably greater for the highest-AOD conditions (r^2 is 0.348 and slope is 0.018) than for the lower-AOD conditions (r^2 is 0.115 and slope is 0.008). This may be due to higher AOD being correlated with more aged smoke which has evolved under stagnation conditions or during prolonged transport. If so, it is possible that this aged aerosol would have longer exposure to the ambient water vapor and thus more time to be influenced by it.

[31] This hypothesis is possibly corroborated when almucantar retrieved single-scattering albedo is examined as a function of column water vapor (Figure 20). For lower-AOD bins there is no significant dependence, while for high AOD the correlation becomes moderately strong and significant at the 99% confidence level (r^2 = 0.36; N = 89), and the trend is toward higher SSA as would be expected for increasingly hydrated aerosol. The differing trends for different AOD bins may be associated with greater coagulation efficiency for conditions of greater aerosol concentration and may explain the monotonic increase of SSA versus CWV slope for the intermediate AOD bins (1.0–1.5 and 1.5–2.0, not pictured).

5.3. Seasonal Volume Size Distribution and Evidence of Dust in the Northern Amazon

[32] Figures 21 and 22 present averaged subsets of size distributions derived for the wet season and the respective peak burning seasons at Alta Floresta and Balbina. For the peak months of biomass burning (August–October in the south and October–December in the north), averaged size distributions are shown for almucantars acquired during the average AOD conditions during these months (in Alta Floresta the dry season AOD_{avg} is 1.0 ± 0.06 [N = 57] and in Balbina the dry season AOD_{avg} is 0.43 ± 0.05 [N =

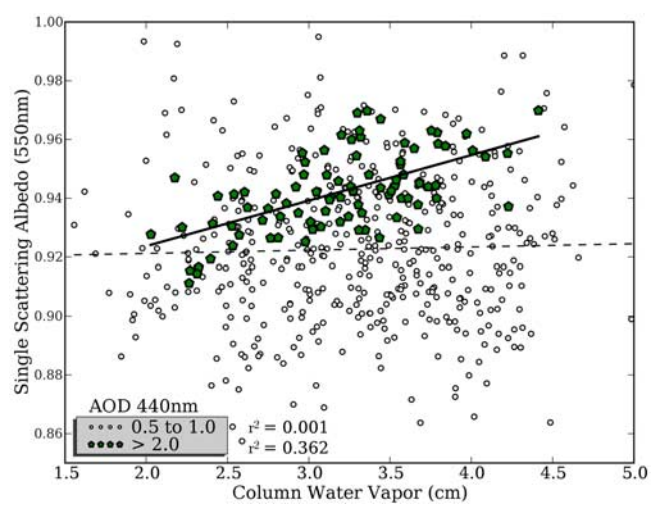

Figure 20. Single-scattering albedo (SSA_{550nm}) as a function of column water vapor for two aerosol optical depth (440 nm) bins.

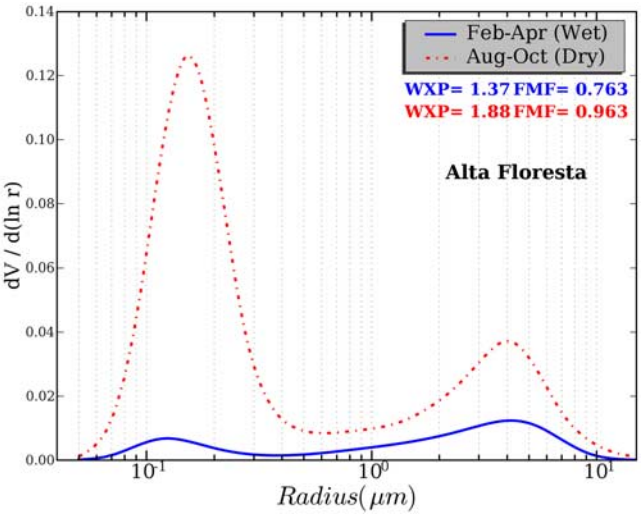

Figure 21. Averaged volume size distributions derived from observations during the wet season (February–April) and the burning season months (August–October) at Alta Floresta.

48]) which may be taken as "typical" size distributions for the burning season in each region. As would be expected, during the burning season the majority of the atmospheric extinction is due to fine mode aerosols, which are responsible for approximately 84% of the total AOD at Balbina and more than 96% of the AOD at Alta Floresta.

[33] The wet season size distributions were derived from observations during the February–April months and are composites of size distributions for all almucantars. Predominantly cloudy conditions at both sites during the wet season limited the availability of days with suitable sky conditions for high-quality almucantar procedures, resulting in a relatively low number of successful retrievals during these months (for Alta Floresta $N = 27$; for Balbina $N = 12$). The aerosol fine mode volume concentrations were at minimal levels during this interval at both locations as would be anticipated. The coarse mode peak concentration is larger for the Balbina site (also observed at Belterra) than in the southern forest, both in absolute terms (0.023 versus 0.012) and relative to the fine mode peak and this factor results in a much lower fine mode fractional contribution to AOD_{440nm} (53%) at Balbina than is observed at Alta Floresta (76%). The peak size of the coarse mode radius for the Balbina site (approximately 1.55 μm) is consistent with the size of desert particles retrieved by AERONET [*Eck et al.*, 2008].

[34] Dust transport to this region during the wet season has been demonstrated previously by satellite [*Koren et al.*, 2006] and in situ sampling (ground and aircraft [*Formenti et al.*, 2001] and aircraft [*Swap et al.*, 1992]). *Swap et al.* [1992] originally noted that considerable amounts of dust observed in the central Amazon basin during the wet season is of Saharan origin, and *Koren et al.* [2006] have documented routine and continuous dust transport from the Sahara to the Amazon basin during the Northern winter. In 1998, the year before our monitoring began, *Formenti et al.* [2001] measured an unbroken 4-day interval of dust at our Balbina site during the same seasonal interval that we observed our dust events and back trajectories conclusively indicated source regions of both the Morrocan coast and the Sahel.

[35] Given the known annual transport of Saharan dust into northeastern South America during this part of the year, it is reasonable to speculate that the enhanced coarse mode for the Balbina site represents a dust signature associated with transport into the Brazilian interior [*Kaufman et al.*, 2005; *Luo et al.*, 2003]. Back trajectory analyses for the dates when the Balbina wet season almucantars were obtained indicated an origination of the aerosol in western Africa for all cases. The very low-average Ångström exponent (0.54) observed in the northern forest during this interval is also consistent with the presence of large (dust-like) aerosol particles.

6. Single-Scattering Albedo Statistics

6.1. Correlation of Aerosol Absorption Properties with Ground Cover Type

[36] A measure of the absorption characteristics of the atmospheric aerosol can also be derived from almucantar sky radiance retrievals for conditions with suitably high-aerosol loadings (greater than 0.4 at 440 nm) and may be quantified as single-scattering albedos at four wavelengths. Early season fires have a greater contribution from grass fires that are characterized by flaming phase combustion which have lower combustion efficiency and produce aerosols with higher-black-carbon content and thus lower single-scattering albedos. As the burning season progresses it would be anticipated that this type of combustion would diminish relative to smoldering-type combustion from woody fuel fires that burn more efficiently and result in higher SSAs. Analyses identified no such seasonal trend in SSA that was statistically significant, however. By a large degree the most robust predictor of the absorption features of smoke aerosols was the ground cover type of the region.

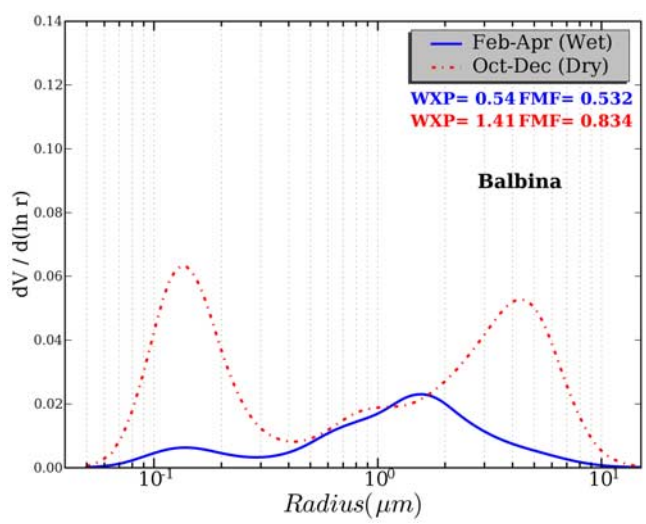

Figure 22. Averaged volume size distributions derived from observations during the wet season (February–April) and the burning season months (October–December) at Balbina.

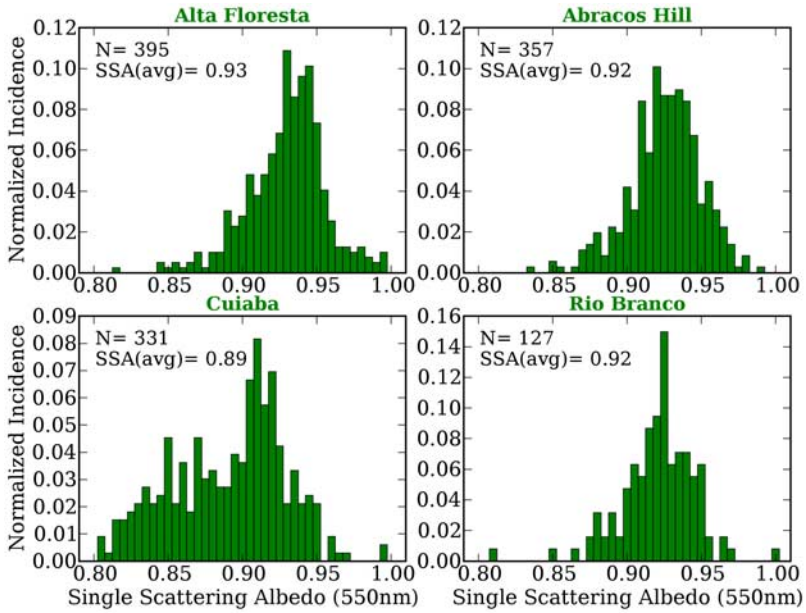

Figure 23. Histograms of single-scattering albedo (SSA_{550nm}) measurements for the southern forest and Cerrado sites (all years combined).

[37] We have a substantial record of single-scattering albedo measurements for the southern forest and Cerrado sites derived from numerous years that are composited (the average of SSA_{440nm} and SSA_{670nm} is shown) and presented as histograms in Figure 23. Regionally averaged values are also presented in Table 2. All of the southern forest sites exhibit similar values of SSA_{550nm} and a moderately absorbing average single-scattering albedo of 0.92–0.93 at 550_{nm}; the northern forest sites average slightly less (0.91), while the Cerrado site (Cuiabá) averages 0.04 less than the southern forest (as we would expect given the difference in predominant fuel for this ground cover type). By definition the Cerrado region includes sites that are primarily influenced by savanna and open pasturelands that exhibit a higher fraction of flaming phase combustion which explains why the mean single-scattering albedo averages substantially less than the mean values in the southern forest region for the corresponding month. The range of SSA is also greater for the Cerrado site (standard deviation is 0.04) than at the three forest sites (approximately 0.025).

[38] This is largely due to the fact that the Cuiabá region experiences significant amounts of smoke from both smoldering and flaming fires as can be seen when the histograms for Alta Floresta and Cuiabá are produced separately for moderate and high-AOD conditions (0.4–0.7 (dark bars in Figure 24) and greater than 1.0 (light bars in Figure 24), respectively). Grass fires (flaming phase combustion) commonly have smaller AODs than forest fires and this results in significantly lower SSA values (average is 0.86) being associated with the smaller AODs at Cuiabá when local savannah fires are prevalent. The higher-AOD conditions are presumably attributable to the transport of forest fire smoke from the north which is reflected in a higher average SSA (average is 0.91) that is more in line with the values observed in the forest region sites. By comparison, Alta Floresta, which is not as strongly influenced by grass fires, exhibits a minimal difference of SSA between the two AOD scenarios (low (0.92) and high (0.93)) which is not surprising for a region where emissions are dominated by biomass burning of tropical forest vegetation. Note that the greater variability of derived SSA for both lower-AOD data sets is partly due to a loss of sensitivity of the inversion algorithm for lower-aerosol loading.

6.2. Comparison With In Situ (Filter-Based) SSA Measurements

[39] *Schmid et al.* [2006] performed in situ measurements of the single-scattering albedo of atmospheric aerosols at the Abracos Hill site during the LBA-SMOCC campaign using a single-wavelength Particle Soot Absorption Photometer (PSAP) (565 nm) and a single-wavelength integrating nephelometer (M903) (545 nm), both manufactured by Radiance Research. Ambient aerosol was sampled and dried prior to particle detection and the uncertainty in measured SSA was estimated as ±0.05 because of errors from particle loss and relative humidity control [*Schmid et al.*, 2006]. Aerosol drying should result in lower SSA, but since the biomass burning aerosol is only weakly hygroscopic this effect should be relatively small. A Cimel Sun Photometer was collocated at the Abracos Hill site during this time. Because the period of study began at the time of year when relatively fewer SSA measurements from the Cimel

Table 2. Statistics for Observed Single-Scattering Albedo (SSA_{550nm}) Grouped by Region (All Years Combined)

	SSA_{550nm}	SD	Number of Alms
Southern forest	0.926	0.026	994
Northern forest	0.914	0.043	129
Cerrado	0.887	0.039	420

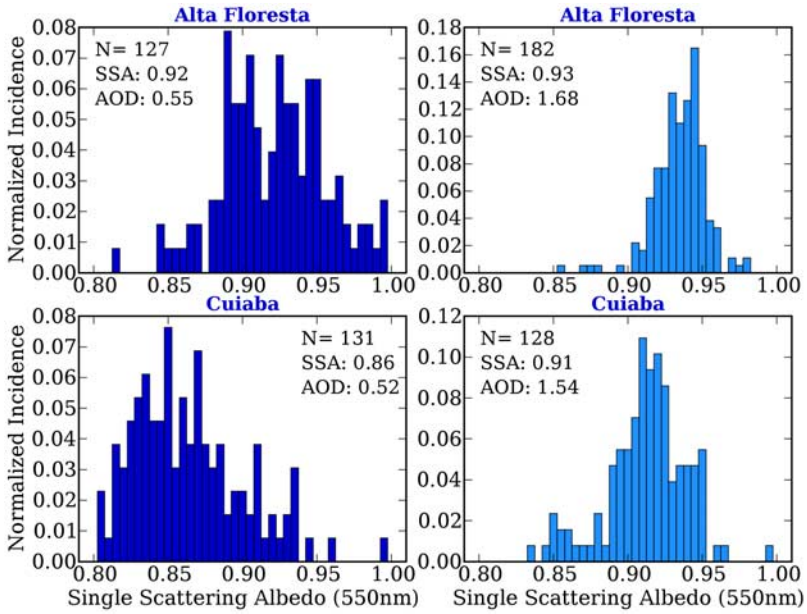

Figure 24. Histograms of single-scattering albedo (SSA_{550nm}) measurements for Alta Floresta and Cuiabá (all years combined) partitioned into two AOD groups (moderate (AOD_{440nm} = 0.4–0.7) plots on the left and high (AOD_{440nm} >1.0) plots on the right).

are acquired, there were only five almucantars during this period that were coincident with the PSAP/M903 observations.

[40] The in situ measurements (1-min sampling) were averaged for a ±30-min interval centered on the time of each Cimel almucantar, and the variability of the SSA from in situ measurements was very small over the hour (average standard deviation of 0.008 with all cases less than 0.014). Although the effective wavelengths of the SSA acquired by the two measurement techniques are slightly different (from Cimel SSA interpolated to 550 nm and from PSAP SSA interpolated to 565 nm), the effect of this spectral difference is trivial. The values of SSA observed by the Cimel exhibited a relatively large range from 0.84 to 0.94 for the five coincident measurements. In general, the agreement was within expectations given the combined uncertainties of the two measurements (±0.03 for the Cimel and ±0.05 for the PSAP/M903) although no significant correlation was observed between the two techniques for the five coincident measurements. The lack of significant correlation is not surprising since the measurement uncertainties are comparable in magnitude to the typical range of the dependent variable during this interval of the year (SSA interquartile range is 0.045). For these five measurements the SMOCC campaign SSA (in situ PSAP) measurements averaged 0.916 ± 0.027, while the corresponding average for the Cimel measurements were 0.902 ± 0.042. The root mean square of the difference in SSA between the ground and columnar measurements was 0.041 with no significant bias (mean difference is −0.014). The discrepancy between the techniques for individual observations of SSA ranged from −0.059 to 0.054 for the five comparisons.

[41] In order to allow for a more expansive comparison the statistics for all daytime in situ SSA measurements (N = 24,011) during the 2002 SMOCC campaign were also compared with those for the set of Cimel almucantars (N = 125) acquired during the corresponding interval (9 September to 14 November) from the full multiyear record of Sun photometer deployment at the site (1999–2006). The agreement between results from the two wholly independent methods was excellent (Cimel is 0.918 ± 0.025 and PSAP is 0.911 ± 0.03) and the histograms of these data are shown in Figure 25. When we average the mean SSA_{550nm} for the 7 years of AERONET (during the SMOCC interval), we get a value of 0.919 with a standard deviation of 0.012, which implies very little year-to-year variation during the campaign period and suggests that it is reasonable to use the multiyear averages for comparison with in situ data during the SMOCC campaign. Although this comparison is not matched in time (includes years other than 2002), it provides further confidence that these techniques are each providing accurate estimates of aerosol absorption within the limits of experimental error.

7. Conclusions

[42] The story of aerosols in the Amazon is largely a tale of two seasons (wet and dry) and the significant interannual variation in aerosol properties is almost entirely a function of the intensity of the biomass burning during the dry season. The atmospheric aerosol regime experienced at a given location is driven by the local land cover type, its proximity to areas of heavy seasonal fires, and regional meteorology. While the aerosol loading (AOD) during wet season months is remarkably consistent at all sites (aside from dust transport events), the southern dry (and transitional) months are most notable for their lack of predictability in part due to the timing and amount of local rainfall and possibly mutable fire management policies (or enforcement vigilance) with the nearest thing to a certainty being the fact that at some point in August the burning will begin.

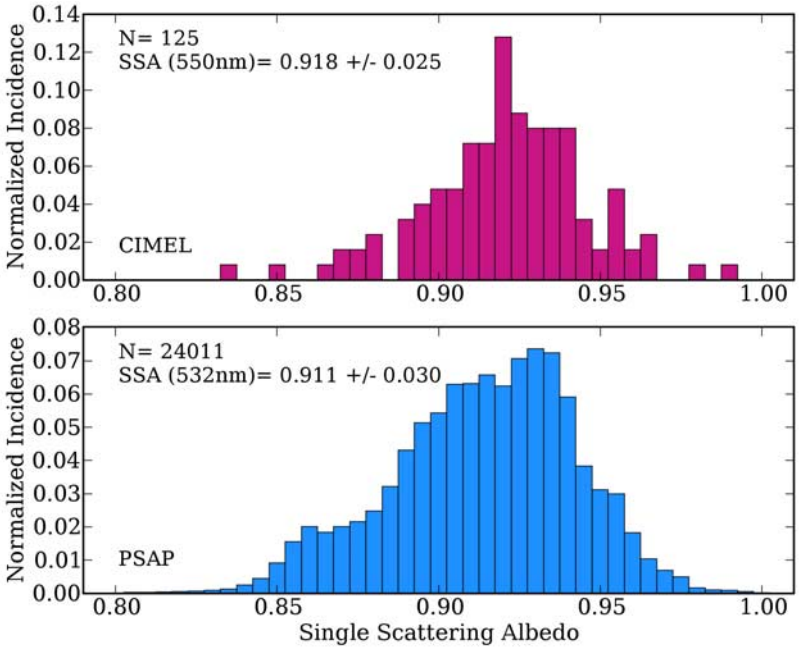

Figure 25. Histograms of single-scattering albedo measurements at Abracos Hill from (top) Cimel almucantars and (bottom) PSAP in situ filter-derived measurements. The interval of comparison was from 9 September to 14 November with PSAP measurements from 2002 and Cimel measurements including almucantars measurements from 1999–2006.

[43] This investigation observed an apparent enhanced hygroscopicity for high-smoke AOD conditions during the burning season that may be associated with aerosol residence time and coagulation effects. Evidence was presented that indicates a likely tendency to underestimate the Ångström exponent because of cloud contamination, at least for certain types of cloud regimes, on the basis of discrepancies between α derived from almucantar and direct Sun measurements. On average this underestimation is not large (approximately 0.1) but may be quite significant for certain observations of α derived from direct Sun measurements. Finally, the highest-AOD events during the wet season clearly suggested the influence of atmospheric mineral dust at the sites in the northern equatorial forest region, likely due to aerosol advected from Western Africa.

[44] **Acknowledgments.** We thank the scientists and technicians responsible for operating and maintaining the instrumentation over the course of many years that generated this high-quality data set and ultimately enabled this paper to be written. These colleagues include Edilson Bernardino de Andrade (Alta Floresta); Alejandro Fonseca Duarte (Rio Branco); José de Souza Nogueira, Edilberto Ojeda de Almeida Filho, and Alfredo Jorge (Cuiabá); Fernando Cardoso, Renata Aguiar, Hemerson Pablo Castro, Rosivaldo Lelis da Silva, and Fabricio Berton Zanchi (Rondônia); Evan Everton (Belterra); and Sr. Zairon (Balbina). Special thanks to the Brazilian scientists that coordinated activities for our subnetwork and ensured that our operations functioned efficiently: Márcia Yamasoe, Aline Procópio, Gilberto Nishioka, and Melina Mara de Andrade Paixão.

References

Anderson, T. L., R. J. Charlson, S. E. Schwartz, R. Knutti, O. Boucher, H. Rodhe, and J. Heintzenberg (2003), Climate forcing by aerosols: A hazy picture, *Science*, *300*, 1103–1104.

Andreae, M. O., et al. (2002), Biogeochemical cycling of carbon, water, energy, trace gases, and aerosols in Amazonia: The LBA-EUSTACH experiments, *J. Geophys. Res.*, *107*(D20), 8066, doi:10.1029/2001JD000524.

Andreae, M. O., D. Rosenfeld, P. Artaxo, A. A. Costa, G. P. Frank, K. M. Longo, and M. A. F. Silva-Dias (2004), Smoking rain clouds over the Amazon, *Science*, *303*(5662), 1337–1342.

Chylek, P., B. Henderson, and M. Mishchenko (2003), Aerosol radiative forcing and the accuracy of satellite aerosol optical depth retrieval, *J. Geophys. Res.*, *108*(D24), 4764, doi:10.1029/2003JD004044.

Dubovik, O., and M. D. King (2000), A flexible inversion algorithm for retrieval of aerosol optical properties from Sun and sky radiance measurements, *J. Geophys. Res.*, *105*(D16), 20,673–20,696.

Dubovik, O., A. Smirnov, B. N. Holben, M. D. King, Y. J. Kaufman, T. F. Eck, and I. Slutsker (2000), Accuracy assessments of aerosol optical properties retrieved from Aerosol Robotic Network (AERONET) Sun and sky radiance measurements, *J. Geophys. Res.*, *105*(D8), 9791–9806.

Dubovik, O., et al. (2006), Application of spheroid models to account for aerosol particle nonsphericity in remote sensing of desert dust, *J. Geophys. Res.*, *111*, D11208, doi:10.1029/2005JD006619.

Eck, T. F., B. N. Holben, I. Slutsker, and A. Setzer (1998), Measurements of irradiance attenuation and estimation of aerosol single scattering albedo for biomass burning aerosols in Amazonia, *J. Geophys. Res.*, *103*(D24), 31,865–31,878.

Eck, T. F., B. N. Holben, J. S. Reid, O. Dubovik, A. Smirnov, N. T. O'Neill, I. Slutsker, and S. Kinne (1999), Wavelength dependence of the optical depth of biomass burning, urban, and desert dust aerosols, *J. Geophys. Res.*, *104*(D24), 31,333–31,349.

Eck, T. F., B. N. Holben, D. E. Ward, O. Dubovik, J. S. Reid, A. Smirnov, M. M. Mukelabai, N. C. Hsu, N. T. O'Neill, and I. Slutsker (2001), Characterization of the optical properties of biomass burning aerosols in Zambia during the 1997 ZIBBEE field campaign, *J. Geophys. Res.*, *106*(D4), 3425–3448.

Eck, T. F., et al. (2003), Variability of biomass burning aerosol optical characteristics in southern Africa during the SAFARI 2000 dry season campaign and a comparison of single scattering albedo estimates from radiometric measurements, *J. Geophys. Res.*, *108*(D13), 8477, doi:10.1029/2002JD002321.

Eck, T. F., et al. (2008), Spatial and temporal variability of column-integrated aerosol optical properties in the southern Arabian Gulf and United Arab Emirates in summer, *J. Geophys. Res.*, *113*, D01204, doi:10.1029/2007JD008944.

Falkovich, A. H., E. R. Graber, G. Schkolnik, Y. Rudich, W. Maenhaut, and P. Artaxo (2005), Low molecular weight organic acids in aerosol particles from Rondonia, Brazil, during the biomass-burning, transition, and wet periods, *Atmos. Chem. Phys.*, *5*, 781–797.

Formenti, P., M. O. Andreae, L. Lange, G. Roberts, J. Cafmeyer, I. Rajta, W. Maenhaut, B. N. Holben, P. Artaxo, and J. Lelieveld (2001), Saharan dust in Brazil and Suriname during the Large-Scale Biosphere-Atmosphere Experiment in Amazonia (LBA) - Cooperative LBA Regional Experiment (CLAIRE) in March 1998, *J. Geophys. Res.*, *106*(D14), 14,919–14,934.

Halthore, R. N., T. F. Eck, B. N. Holben, and B. L. Markham (1997), Sun photometric measurements of atmospheric water vapor column abundance in the 940-nm band, *J. Geophys. Res.*, *102*(D4), 4343–4352.

Holben, B. N., A. Setzer, T. F. Eck, A. Pereira, and I. Slutsker (1996), Effect of dry-season biomass burning on Amazon basin aerosol concentrations and optical properties, 1992–1994, *J. Geophys. Res.*, *101*(D14), 19,465–19,482.

Holben, B. N., et al. (1998), AERONET: A federated instrument network and data archive for aerosol characterization, *Remote Sens. Environ.*, *66*, 1–16.

Holben, B. N., et al. (2001), An emerging ground-based aerosol climatology: Aerosol optical depth from AERONET, *J. Geophys. Res.*, *106*(D11), 12,067–12,097.

Holben, B. N., T. F. Eck, I. Slutsker, A. Smirnov, A. Sinyuk, J. Schafer, D. Giles, O. Dubovik (2006), AERONET's Version 2.0 quality assurance criteria, in *Remote Sensing of Atmosphere and Clouds*, edited by S.-C. Tsay et al. *Proc. SPIE,* 6408, 64080Q, doi:10.1117/12.706524.

Jethva, H., S. K. Satheesh, and J. Srinivasan (2005), Seasonal variability of aerosols over the Indo-Gangetic basin, *J. Geophys. Res.*, *110*, D21204, doi:10.1029/2005JD005938.

Kaufman, Y. J., I. Koren, L. A. Remer, D. Tanré, P. Ginoux, and S. Fan (2005), Dust transport and deposition observed from the Terra-Moderate Resolution Imaging Spectroradiometer (MODIS) spacecraft over the Atlantic Ocean, *J. Geophys. Res.*, *110*, D10S12, doi:10.1029/2003JD004436.

Kinne, S., et al. (2003), Monthly averages of aerosol properties: A global comparison among models, satellite data, and AERONET ground data, *J. Geophys. Res.*, *108*(D20), 4634, doi:10.1029/2001JD001253.

Koren, I., Y. J. Kaufman, L. A. Remer, and J. V. Martins (2004), Measurement of the effect of Amazon smoke on inhibition of cloud formation, *Science*, *303*(5662), 1342–1345.

Koren, I., Y. J. Kaufman, R. Washington, M. C. Todd, Y. Rudich, J. V. Martins, and D. Rosenfeld (2006), The Bodélé depression: A single spot in the Sahara that provides most of the mineral dust to the Amazon forest, *Environ. Res. Lett.*, *1*(014005), doi:10.1088/1748-9326/1/1/014005.

Kotchenruther, R. A., and P. V. Hobbs (1998), Humidification factors of aerosols from biomass burning in Brazil, *J. Geophys. Res.*, *103*(D24), 32,081–32,090.

Liu, H., R. T. Pinker, and B. N. Holben (2005), A global view of aerosols from merged transport models, satellite, and ground observations, *J. Geophys. Res.*, *110*, D10S15, doi:10.1029/2004JD004695.

Luo, C., N. M. Mahowald, and J. del Corral (2003), Sensitivity study of meteorological parameters on mineral aerosol mobilization, transport, and distribution, *J. Geophys. Res.*, *108*(D15), 4447, doi:10.1029/2003JD003483.

Mircea, M., et al. (2005), Importance of the organic aerosol fraction for modeling aerosol hygroscopic growth and activation: A case study in the Amazon Basin, *Atmos. Chem. Phys.*, *5*, 3111–3126.

Raj, P. E., P. C. S. Devara, R. S. Maheskumar, G. Pandithurai, K. K. Dani, S. K. Saha, S. M. Sonbawne, and Y. K. Tiwari (2004), Results of sun photometer-derived precipitable water content over a tropical Indian station, *J. Appl. Meteorol.*, *43*(10), 1452–1459.

Reid, J. S., P. V. Hobbs, R. J. Ferek, D. R. Blake, J. V. Martins, M. R. Dunlap, and C. Liousse (1998), Physical, chemical, and optical properties of regional hazes dominated by smoke in Brazil, *J. Geophys. Res.*, *103*(D24), 32,059–32,080.

Reid, J. S., T. F. Eck, S. A. Christopher, P. V. Hobbs, and B. Holben (1999), Use of the Ångstrom exponent to estimate the variability of optical and physical properties of aging smoke particles in Brazil, *J. Geophys. Res.*, *104*(D22), 27,473–27,489.

Rissler, J., A. Vestin, E. Swietlicki, G. Fisch, J. Zhou, P. Artaxo, and M. O. Andreae (2006), Size distribution and hygroscopic properties of aerosol particles from dry-season biomass burning in Amazonia, *Atmos. Chem. Phys.*, *6*, 471–491.

Schmid, B., et al. (2001), Comparison of Columnar water-vapor measurements from solar transmittance methods, *Appl. Opt.*, *40*, 1886–1896.

Schmid, O., P. Artaxo, W. P. Arnott, D. Chand, L. V. Gatti, G. P. Frank, A. Hoffer, M. Schnaiter, and M. O. Andreae (2006), Spectral light absorption by ambient aerosols influenced by biomass burning in the Amazon Basin: part I: Comparison and field calibration of absorption measurement techniques, *Atmos. Chem. Phys.*, *6*, 3443–3462.

Silva Dias, M. A. F., et al. (2002), A case study of convective organization into precipitating lines in the Southwest Amazon during the WETAMC and TRMM-LBA, *J. Geophys. Res.*, *107*(D20), 8078, doi:10.1029/2001JD000375.

Smirnov, A., B. N. Holben, T. F. Eck, O. Dubovik, and I. Slutsker (2000), Cloud-screening and quality control algorithms for the AERONET database, *Remote Sens. Environ.*, *73*(3), 337–349.

Smirnov, A., B. N. Holben, A. Lyapustin, I. Slutsker and T. F. Eck (2004), AERONET processing algorithm refinement, paper presented at AERONET Workshop, Univ. of Huelva and the Span. Soc. of Optics, El Arenosillo, Spain, May 10–14, 2004.

Swap, R., M. Garstang, S. Greco, R. Talbot, and P. Kållberg (1992), Saharan dust in the Amazon Basin, *Tellus B*, *44*(2), 133–149, doi:10.1034/j.1600-0889.1992.t01-1-00005.x.

Vermote, E. F., D. Tanre, J. L. Deuze, M. Herman, and J. J. Morcrette (1997), Second simulation of the satellite signal in the solar spectrum, 6S: An overview, *IEEE Trans. Geosci. Remote Sens.*, *35*, 675–686.

Yu, H., R. E. Dickinson, M. Chin, Y. J. Kaufman, B. N. Holben, I. V. Geogdzhayev, and M. I. Mishchenko (2003), Annual cycle of global distributions of aerosol optical depth from integration of MODIS retrievals and GOCART model simulations, *J. Geophys. Res.*, *108*(D3), 4128, doi:10.1029/2002JD002717.

P. Artaxo, Departamento de Física Aplicada, Instituto de Física, Universidade de São Paulo, Rua do Matão, Travessa R, 187, Caixa Postal 66318, São Paulo, SP-05508-900, Brazil.

A. F. Duarte, Departamento de Ciencias da Natureza, Universidade Federal do Acre, BR 364, Km 04, Rio Branco, AC-69.915-900, Brazil.

T. F. Eck and B. N. Holben, Biospheric Sciences Branch, NASA Goddard Space Flight Center, Code 923, Greenbelt, MD 20771, USA.

J. S. Schafer, Science Systems and Applications, Inc., 10210 Greenbelt Road, Suite 600 Lanham, MD 20706, USA. (joel.schafer@nasa.gov)